Biochemistry

Bisindolylmaleimide Ligands Stabilize *c-MYC* G-Quadruplex DNA Structure and Downregulate Gene Expression

Satendra Kumar, Rajesh Kumar Reddy Sannapureddi, Chaitra S. Todankar, R. Ramanathan, Annyesha Biswas, Bharathwaj Sathyamoorthy,* and P. I. Pradeepkumar*

Read Online

ACCESS | Metrics & More | Article Recommendations | Supporting Information

ABSTRACT: G-Quadruplex (G4) structures play a pivotal role in diverse biological functions, including essential processes, such as telomere maintenance and gene regulation. G4 structures formed in functional regions of genomes are actively pursued toward therapeutics and are targeted by small-molecule ligands that alter their structure and/or stability. Herein, we report the synthesis of bisindolylmaleimide-based (**BIM**) ligands, which preferentially stabilize parallel G4 structures of *c-MYC* and *c-KIT* oncogenes over the telomeric *h-RAS1* G4 and duplex DNAs. The preferential stabilization of parallel G4s with **BIM** ligands is further validated by the DNA polymerase stop assay, where stop products were only observed for templates containing the *c-MYC* G4 sequence. Nuclear magnetic resonance (NMR) titration studies indicate that the lead ligand **BIM-Pr1** forms a 2:1 complex with *c-MYC* G4 DNA with a K_D of 38 ± 5 μM. The **BIM** ligand stacks at the 5′ and 3′ quartets, with molecular modeling and dynamics studies supporting the proposed binding mode. The ligand is cytotoxic to HeLa cells and downregulates *c-MYC* gene expression. Collectively, the results present bisindolylmaleimide scaffolds as novel and powerful G4 targeting agents.
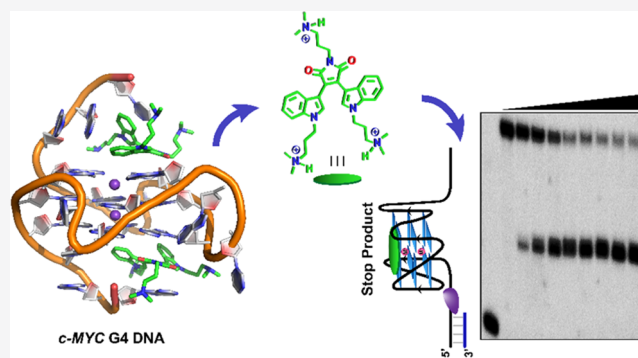
INTRODUCTION

DNA can form noncanonical secondary structures such as G-quadruplex (G4), i-motif, hairpin, triplexes, etc.[1] G4 structures have gained profound attention as they harbor various biological functions. Putative G4 forming sequences are present in the telomeric region, the promoter region of various protooncogenes, and the untranslated region of mRNAs and are observed in the immunoglobulin switch regions.[2,3] Due to their dynamic nature, these structures can sample parallel, hybrid (3 + 1), and antiparallel topologies depending on the type and size of the loop, glycosyl dihedral angle, nucleotide chain length, and nature of metal ions.[4,5] The human telomeric G4 sequence exhibits polymorphism across parallel, hybrid (3 + 1), and antiparallel topologies modulated by metal ions and molecular crowding agents.[5] On the other hand, putative G4 forming sequences at the promoter regions (*c-MYC*, *c-KIT*, *BCL-2*, *VEGF*, *HIF-1α*, *PDGF*, *RET*, etc.) get folded into a parallel topology *in vitro* in the presence of K⁺ ions.[6−9] G4 structures play a crucial role in the inhibition of telomerase activity, downregulation of replication, and modulating gene expression.[3−5] Therefore, stabilization of these G4 structures by exogenous small molecules has been harnessed to develop anticancer agents.[10,11]

Over the years, several molecule/ligands have been reported to stabilize G4 structures,[11−15] preferentially over duplex DNA.

However, accomplishing specificity for a given topology across the myriad G4 topologies has remained challenging owing to similar G-quartet interfaces.[16] Therefore, designing ligands that can proficiently discriminate between various G4 topologies is a fascinating and active field of research.

In continuation of the ongoing efforts, our group has reported indeno-pyrimidine derivatives,[17] bisbenzimidazole carboxamide derivatives,[18] indolylmethyleneindanone,[19] and benzothiazole hydrazones of furylbenzamide-based derivatives[20] showing specific stabilization of parallel promoter *c-KIT* and *c-MYC* G4 structures over various topologies of telomeric and duplex DNAs.[21] However, the in-cell behavior of these ligands is yet to be explored. Here, we report the bisindolemaleimide (**BIM**)-based ligands comprising cationic side chains of different lengths as G4 stabilizers (Figure 1).

Ligand-induced preferential stabilization of *c-MYC* and *c-KIT* G4 DNAs was explored using thermal melting studies with circular dichroism (CD) spectroscopy, titration studies with
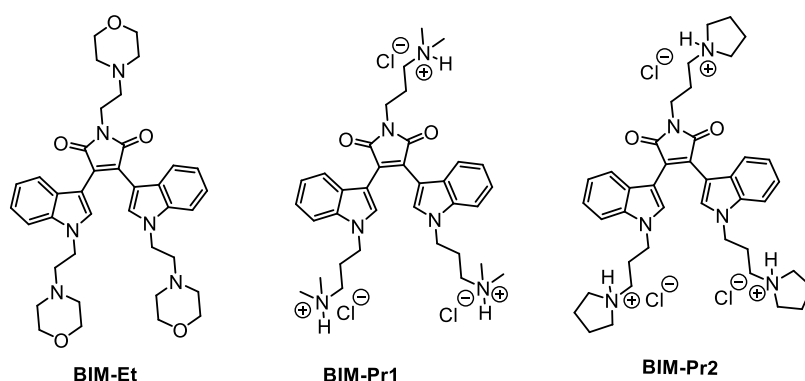
Figure 1. Structures of ligands **BIM-Et, BIM-Pr1,** and **BIM-Pr2** containing a bisindolylmaleimide core with cationic amine side chains.

CD and solution-state nuclear magnetic resonance (NMR) spectroscopy, and a DNA polymerase stop assay. Cell-based assays evaluate the effect of the lead ligand on *c-MYC* gene expression. Furthermore, molecular modeling and dynamics studies provide atomistic details of the binding interaction of the ligand with the *c-MYC* G4 structure.

EXPERIMENTAL SECTION

General Methods. All chemicals, reagents, and solvents were purchased from Merck, Spectrochem, Finar, and TCI. Commercially available acetonitrile and dichloromethane were dried using calcium hydride, while DMF and THF solvents were kept overnight in molecular sieves (4 Å) under a N_2 atmosphere. Thin-layer chromatography (TLC) was performed on silica gel plates precoated with fluorescent indicators and visualized under UV light (260 nm). Silica gel (100−200 mesh) and basic or neutral alumina (60−325 mesh) were used in column chromatography to purify the compounds. ^1H NMR and ^{13}C NMR spectra were recorded on 400 MHz and 500 MHz NMR instruments (Bruker). Chemical shifts (δ) in parts per million were referenced to the residual signal of TMS (0 ppm) or the residual proton signal from deuterated solvents: $CDCl_3$ (7.26 ppm), CD_3OD (3.31 ppm), or DMSO-d_6 (2.5 ppm) for ^1H NMR spectra; and $CDCl_3$ (77.2 ppm), CD_3OD (49.1 ppm), and DMSO-d_6 (39.5 ppm) for ^{13}C NMR spectra. Multiplicities of ^1H NMR spin couplings are recounted as s (singlet), d (doublet), t (triplet), q (quartet), and m (multiplet and overlapping spin systems). Values for apparent coupling constants (J) were reported in hertz. High-resolution mass spectra (HRMS) were recorded in the positive ion electrospray ionization (ESI) mode using a Q-TOF analyzer. Human cervical cancer (HeLa) cell lines and human embryonic kidney (Lenti-X) cell lines were acquired from NCCS, Pune. The enzymes (*Taq* DNA polymerase, PNK), dNTPs, GeneJET RNA purification kit, and verso cDNA synthesis kit were purchased from Thermo Fisher Scientific. Brilliant III Ultra-Fast SYBR green qPCR Master Mix was purchased from Agilent Technologies. All of the media, serum, antibiotics, and reagents used for cell-based experiments were purchased from HiMedia, MP Biomedicals, and Gibco. The reagent used for the cytotoxicity assay, CellTiter-Glo, was purchased from Promega.

Synthetic Procedures. *1-(2-Morpholinoethyl)-3,4-bis(1-(2-morpholinoethyl)-1H-indol-3-yl)-1H-pyrrole-2,5-dione* **(BIM-Et).** To a stirred solution of bisindolylmaleimide (100 mg, 0.30 mmol) and Cs_2CO_3 (497 mg, 1.5 mmol) in dry THF, 4-(2-chloroethyl) morpholine hydrochloride (284 mg 1.5

mmol) was added at room temperature, and the reaction mixture was heated at 70 °C temperature for 1 h under microwave radiation (250 W). After completion of the reaction, the mixture was cooled to room temperature and extracted with EtOAc. The organic layer was washed with brine solution and dried over anhydrous Na_2SO_4. After this, the excess solvent was evaporated under reduced pressure; column chromatography (5% MeOH in DCM) was done using neutral alumina to obtain a pure red solid compound **BIM-Et.** Yield: 40% (81 mg); R_f = 0.4 (10% MeOH in DCM); ^1H NMR (400 MHz, $CDCl_3$) δ 7.75 (s, 2H), 7.30 (d, J = 8.2 Hz, 2H), 7.10−7.00 (m, 2H), 6.94 (d, J = 8.0 Hz, 2H), 6.73−6.69 (m, 2H), 4.25 (t, J = 6.7 Hz, 4H), 3.81 (t, J = 6.6 Hz, 2H), 3.71−3.66 (m, 12H), 2.74 (t, J = 6.8 Hz, 4H), 2.66 (t, J = 6.6 Hz, 2H), 2.56 (bs, 4H), 2.46 (t, J = 4.5 Hz, 8H); ^{13}C NMR (100 MHz, DMSO-d_6) δ 172.5, 136.3, 132.2 127.0, 126.4, 122.5, 122.3, 120.1, 109.5, 106.3, 67.2, 67.0, 58.0, 56.6, 53.9, 53.7, 44.3, 35.3; HRMS (ESI): m/z calcd for $C_{38}H_{47}N_6O_5$ [M + H]$^+$ 667.3601; found, 667.3602 (Δm = +0.0001 and error = +0.2 ppm).

3,3′-((1-(3-(Dimethylammonio)propyl)-2,5-dioxo-2,5-di-hydro-1H-pyrrole-3,4-diyl)bis(1H-indole-3,1-diyl))bis(N,N-di-methylpropan-1-aminium) (2). To a stirred solution of compound **1** (100 mg, 0.30 mmol) and Cs_2CO_3 (488.5 mg, 1.5 mmol) in dry THF, 3-dimethylamino-1-propyl chloride hydrochloride (237.0 mg, 1.5 mmol) was added at room temperature, and the reaction mixture was heated at 70 °C for 1 h under microwave radiation (250 W). After completion of the reaction, the mixture was cooled to room temperature and extracted with EtOAc. The organic layer was washed with brine solution and dried over anhydrous Na_2SO_4. After that, the excess solvent was evaporated under reduced pressure, and column chromatography (5% MeOH in DCM) was done using neutral alumina to obtain a pure red sticky solid compound **2.** Yield: 26% (46 mg); R_f = 0.4 (10% MeOH in DCM); ^1H NMR (400 MHz, $CDCl_3$) δ 7.67 (s, 2H), 7.30 (d, J = 8.2 Hz, 2H), 7.07−7.02 (m, 2H), 6.95 (d, J = 8.0 Hz, 2H), 6.73−6.68 (m, 2H), 4.18 (t, J = 6.8 Hz, 4H), 3.72 (t, J = 7.1 Hz, 2H), 2.37 (t, J = 7.3 Hz, 2H), 2.23−2.18 (m, 22H), 1.96−1.84 (m, 6H); ^{13}C NMR (100 MHz, $CDCl_3$) δ 172.5, 136.2, 131.8 126.7, 126.2, 122.2, 122.0, 119.8, 109.6, 105.9, 57.1, 56.1, 45.4, 45.4, 44.2, 36.4, 27.9, 27.0; HRMS (ESI): m/z calcd for $C_{35}H_{47}N_6O_2$ [M + H]$^+$ 583.3765; found, 583.3757 (Δm = −0.0008 and error = −1.3 ppm).

3,3′-((1-(3-(Dimethylammonio)propyl)-2,5-dioxo-2,5-di-hydro-1H-pyrrole-3,4-diyl) bis(1H-indole-3,1-diyl))bis(N,N-dimethylpropan-1-aminium)·3HCl (BIM-Pr1). To a stirred

solution of compound **2** (15 mg, 0.02 mmol) in DCM, one drop of concentrated HCl was added, and the reaction mixture was stirred at room temperature for 6 h. After that, the excess solvent was evaporated under reduced pressure. The resultant product was washed with diethyl ether to get a protonated pure red solid **BIM-Pr1**. Yield: 68% (12 mg); R_f = 0.3 (15% MeOH in DCM); ^{1}H NMR (400 MHz, DMSO-d_6) δ 10.82 (bs, 2H), 10.46 (bs, 1H), 7.90 (s, 2H), 7.57 (d, J = 8.3 Hz, 2H), 7.11−7.07 (m, 2H), 6.87 (d, J = 8.0 Hz, 2H), 6.76 (t, J = 7.4 Hz, 2H), 4.37 (t, J = 7 Hz, 4H), 3.64 (t, J = 6.4 Hz, 2H), 3.15−3.10 (m, 2H), 3.04−2.98 (m, 4H), 2.74−2.68 (m, 18H), 2.20−2.10 (m, 4H), 2.08−1.99 (m, 2H); ^{13}C NMR (100 MHz, DMSO-d_6) δ 171.4, 135.7, 132.0 126.7, 125.6, 122.0, 121.4, 119.8, 110.3, 105.2, 54.2, 53.8, 43.0, 42.0, 41.9, 35.0, 24.6, 23.6; HRMS (ESI): m/z calcd for $C_{35}H_{49}N_6O_2$ [M/3]$^+$ 195.1300; found, 195.1303 (Δm = −0.0003 and error = −1.6 ppm).

1-(3-Bromopropyl)-3,4-bis(1-(3-bromopropyl)-1H-indol-3-yl)-1H-pyrrole-2,5-dione (3). To a stirred solution of compound **1** (100 mg, 0.30 mmol) and Cs_2CO_3 (488 mg, 1.5 mmol) in dry THF, 1,3-dibromopropane (301.8 mg, 1.8 mmol) was added at room temperature, and the reaction mixture was heated at 70 °C for 1 h under the microwave condition (250 W). After completion of the reaction, it was cooled to room temperature and extracted with EtOAc. The organic layer was washed with brine solution and dried over anhydrous Na_2SO_4. The obtained red solid was utilized in the next step without any further purification to obtain compound **4**.

1,1′-(((2,5-Dioxo-1-(3-(pyrrolidin-1-ium-1-yl)propyl)-2,5-dihydro-1H-pyrrole-3,4-diyl)bis(1H-indole-3,1-diyl))bis-(propane-3,1-diyl))bis(pyrrolidin-1-ium) (4). To a stirred solution of crude compound **3** (100 mg, 0.14 mmol) in dry THF, pyrrolidine (103 mg, 1.4 mmol) was added dropwise, and the reaction mixture was heated at 60 °C for 12 h. After completion of the reaction, the excess solvent was evaporated under reduced pressure and column chromatography (6% MeOH in DCM) was done using neutral alumina to obtain a pure red sticky solid compound **8**. Yield: 36% (55 mg); R_f = 0.3 (12% MeOH in DCM); ^{1}H NMR (500 MHz, CDCl$_3$) δ 7.68 (s, 2H), 7.31 (d, J = 8.2 Hz, 2H), 7.05 (t, J = 7.2 Hz, 2H), 6.94 (d, J = 8.0 Hz, 2H), 6.70 (t, J = 7.5 Hz, 2H), 4.22 (t, J = 6.8 Hz, 4H), 3.74 (t, J = 7.0 Hz, 2H), 2.57−2.38 (m, 18H), 2.04−1.90 (m, 6H), 1.77−1.74 (m, 12H); ^{13}C NMR (125 MHz, CDCl$_3$) δ 172.7, 136.3, 131.8, 126.8, 126.4, 122.4, 122.1, 120.0, 109.7, 106.1, 54.3, 54.2, 54.1, 53.0, 44.7, 36.8, 29.4, 28.3, 23.6, 23.6; HRMS (ESI): m/z calcd for $C_{41}H_{53}N_6O_2$ [M + H]$^+$ 661.4235; found, 661.4238 (Δm = +0.0003 and error = +0.4 ppm).

1,1′-(((2,5-Dioxo-1-(3-(pyrrolidin-1-ium-1-yl)propyl)-2,5-dihydro-1H-pyrrole-3,4-diyl)bis(1H-indole-3,1-diyl))bis-(propane-3,1-diyl))bis(pyrrolidin-1-ium)·3HCl (BIM-Pr2). To a stirred solution of compound **4** (15 mg, 0.02 mmol) in DCM, one drop of concentrated HCl was added, and the reaction mixture was stirred at room temperature for 6 h. After that, the excess solvent was evaporated under reduced pressure. The resultant product was washed with diethyl ether to get a protonated pure red solid **BIM-Pr2**; Yield 70% (11 mg); R_f = 0.3 (15% MeOH in DCM); ^{1}H NMR (400 MHz, D$_2$O) δ 7.54 (s, 2H), 7.37 (d, J = 8.3 Hz, 2H), 7.06 (t, J = 7.5 Hz, 2H), 6.73 (d, J = 7.5 Hz, 2H), 6.63 (t, J = 7.3 Hz, 2H), 4.16 (t, J = 6.6 Hz, 4H), 3.58−3.52 (m, 4H), 3.13 (t, J = 7.1 Hz, 2H), 2.93−2.91 (m, 6H), 2.77−2.76 (m, 4H), 2.08−

1.80 (m, 22H); ^{13}C NMR (100 MHz, D$_2$O) δ 173.5, 136.0, 131.9 127.5, 125.6, 122.6, 121.4, 120.3, 110.2, 105.2, 54.2, 54.1, 52.5, 52.1, 43.1, 35.0, 26.1, 25.0, 22.5; HRMS (ESI): m/z calcd for $C_{41}H_{55}N_6O_2$ [M/3]$^+$ 221.1457; found, 221.1455 (Δm = +0.0002 and error = +0.8 ppm).

Preparation of the Stock Solution of Ligands. A 5 mM stock solution of **BIM-Et** was prepared in DMSO, whereas **BIM-Pr1** and **BIM-Pr2** were dissolved in H$_2$O.

Oligonucleotides. The DNA oligonucleotide sequences used in all of the studies are mentioned in Table S3. Crude oligonucleotides were obtained from IDT (Belgium) and Sangon (China) in the desalted form. They were purified using 20% PAGE (7 M urea) using standard protocols.[22] Purified oligonucleotides were further eluted via desalting the Sep-Pak column. DNA oligonucleotides were dissolved in water, and their respective absorbances were measured at 260 nm wavelength in a Perkin Elmer Lambda Bio$^+$ UV−vis spectrophotometer. Then, the concentrations of all of the oligonucleotides were evaluated using appropriate molar extinction coefficients (ε) obtained from nearest neighbor models.

CD Titration Studies. CD titration experiments were carried out in a Jasco-1500 CD spectrometer using a scan speed of 100 nm/min with a response time of 4 s at 25 °C. All spectra were recorded from the 200−340 nm wavelength range using 1 mm path length of a quartz cuvette. In the presence of the added salt, the CD spectra were measured using 10 μM oligonucleotide in 10 mM lithium cacodylate buffer conditions at 7.2 pH. The entire DNA solution in the buffer was equilibrated at room temperature for 3 min after addition of each ligand concentration. The baseline was measured in 10 mM lithium cacodylate buffer at 7.2 pH. Each spectrum is an average of three consecutive measurements. All spectra were analyzed with Origin 8.0 software.

CD Melting Studies. Thermal melting experiments with CD were carried out in a Jasco-1500 spectrometer having a quartz cuvette of 1 mm path length at a heating rate of 1 °C min^{-1}. Then, 15 μM of duplex and 10 μM of G4 forming DNA solution consisting of 10 mM lithium cacodylate buffer of pH 7.2 along with the appropriate salt concentration were annealed by heating at 95 °C for 5 min followed by slow cooling to room temperature over a period of 4−6 h. A total of 90 mM LiCl and 10 mM KCl were used for telomeric, c-*KIT1,* and duplex DNA, 99 mM LiCl and 1 mM KCl were used for c-*MYC,* whereas for h-*RAS1,* 50 mM LiCl and 50 mM KCl were used. After annealing, 5 molar equiv of the ligand was added to the annealed DNA solutions and then incubated overnight at 4 °C temperature. Thermal melting spectra were monitored at 263 nm for c-*MYC* and c-*KIT1* G4 DNA. For h-*RAS1,* telomeric, and duplex DNA, thermal melting profiles were performed at 290, 295, and 242 nm, respectively. The melting temperature was measured from the characteristic sigmoidal curve by fitting in the Boltzmann function obeying the following equation in Origin 8.0 software.[23]

$$\theta = \theta_{min} + (\theta_{max} - \theta_{min})/(1 + \exp((T_{1/2} - T)/s))$$

where θ refers to the ellipticity; θ_{min} and θ_{max} are the minimum and maximum θ, respectively; T is temperature; $T_{1/2}$ is the melting temperature; and s is a fitting parameter.

NMR Titration Studies. The c-*MYC* DNA oligomer was synthesized in-house using the K&A H8 oligosynthesizer, cleaved, and deprotected with a 1:1 ammonia/methylamine solution. The synthesized oligonucleotide was then desalted

with Sep-pak columns as reported before.[24] DNA solution (at 100 μM monomer concentration) was heated at 95 °C for 5 min to ensure maximal unfolding. Subsequently, a 25 mM potassium phosphate buffer (pH 7.0) and 70 mM KCl solution was added to this DNA solution and was heated at 95 °C for an additional 5 min. Following this, the sample was allowed to anneal at room temperature (298 K) overnight. The annealed solution was then concentrated to 1 mM DNA concentration using 3 kDa centrifugal filters spun at 4000g (4 °C) for 30 min. Buffer exchange was performed with a centrifugal filter, with the concentration from 15 to ∼0.5 mL repeated 4 times to equilibrate the sample in NMR buffer. The final sample contained 100 μM DNA in a 300 μL volume along with 5% v/v D_2O (for field-frequency locking) and 50 μM trimethylsilylpropanoic acid (TSP, for chemical shift referencing purposes) in a 5 mm medium-wall NMR tube (I.D. = 3.43 mm, Norell Inc.). The **BIM-Pr1** ligand that was to be titrated was prepared as a 30 mM stock solution in the DMSO-d_6 solvent. The NMR sample was titrated with the **BIM-Pr1** ligand stock solution by addition of the ligand in a serial fashion, within the same NMR tube. Considering the intermediate-fast exchange time scale of ligand binding, the titrated solution was allowed to equilibrate for a period of 10 min before acquisition of ^{1}H-1D NMR data.

Data were acquired at 0.5, 1.0, 2.0, 4.0, 5.0, 6.0, 8.0, and 10.0 molar equiv of the **BIM-Pr1** ligand. The total concentration of DMSO-d_6 present in the solution after 10 molar equiv titration was estimated to be ∼3.5% v/v. All of the data were acquired at 298 K using a 700 MHz spectrometer equipped with AVANCE III console and a triple channel inverse detect cryogenically cooled probe with z-gradient shims. Spectra were processed and analyzed with topspin v4.0.6. ^{1}H chemical shifts were referenced to the internal standard (TSP), and ^{1}H chemical shift perturbations (CSPs) were determined with respect to the control (0 eq **BIM-Pr1**) sample.

Binding Model and NMR Chemical Shift Analysis. Two-site independent binding analysis was modeled to estimate the dissociation constant K_D. Equations that were previously deduced for fitting two independent binding sites of the ligand to protein complexes[25] were adapted. Two assumptions were introduced into the model based on the data acquired (see the manuscript), namely: (a) affinity at both sites of 5′- and 3′-planes was assumed to be equal ($K_{D1} = K_{D2}$), and (b) no CSP for 5′-plane (or 3′-plane) nucleotides due to ligand binding on the 3′-plane (or 5′-plane). Chemical shift perturbations experienced by the spins in middle-plane nucleotides are the same due to binding in the 5′- and 3′-planes.

The equations involving dissociation constants (K_{D1} and K_{D2}), ligand concentration ([L]), and fraction of the different states (f_F, $f_{5'B}$, $f_{3'B}$, and $f_{(5'+3')B}$ are fraction of folded, 5′-plane ligand bound, 3′-plane bound, and both planes bound states, respectively) are listed below. These equations reported for proteins[25] were adapted for the *c-MYC* G4 system.

$$f_F = \frac{K_{D1}K_{D2}}{K_{D1}K_{D2} + (K_{D1} + K_{D2})[L] + [L]^2}$$

$$f_{5'B} = \frac{K_{D2}[L]}{K_{D1}K_{D2} + (K_{D1} + K_{D2})[L] + [L]^2}$$

$$f_{3'B} = \frac{K_{D1}[L]}{K_{D1}K_{D2} + (K_{D1} + K_{D2})[L] + [L]^2}$$

$$f_{(5'+3')B} = \frac{[L]^2}{K_{D1}K_{D2} + (K_{D1} + K_{D2})[L] + [L]^2}$$

The following equations are obtained by rearranging the above to determine chemical shift perturbations ($\Delta\delta_{obs}$) as a function of the ligand ([L]) and the DNA concentration ([D]), with $[D]_{tot}$ and $[L]_{tot}$ being the total DNA and ligand concentrations, respectively.

$$[L]^3 + a[L]^2 + b[L] + c = 0$$

$$a = 2[D]_{tot} - [L]_{tot} + K_{D1} + K_{D2}$$

$$b = ([D]_{tot} - [L]_{tot})(K_{D1} + K_{D2}) + K_{D1}K_{D2}$$

$$c = -K_{D1}K_{D2}[L]_{tot}$$

$$[L] = \frac{-a}{3} + \frac{2}{3}\sqrt{(a^2 - 3b)}\cos\frac{\theta}{3}\text{where }\theta$$
$$= \arccos\frac{-2a^3 + 9ab - 27c}{2\sqrt{(a^2 - 3b)^3}}$$

NMR chemical shift differences are given by

$$\Delta\delta_{obs} = \frac{[5'B] + [(5' + 3')B]}{[D]_{tot}}\Delta\delta_{5'B}$$
$$+ \frac{[3'B] + [(5' + 3')B]}{[D]_{tot}}\Delta\delta_{3'B}$$
$$= (f_{5'B} + f_{(5'+3')B})\Delta\delta_{5'B} + (f_{3'B} + f_{(5'+3')B})\Delta\delta_{3'B}$$
$$= \frac{[L]}{K_{D1} + [L]}\Delta\delta_{5'B} + \frac{[L]}{K_{D2} + [L]}\Delta\delta_{3'B}$$

[5′B], [3′B], and [(5′ + 3′)B] are concentrations of 5′B, 3′B, and (5′ + 3′)B forms, respectively, and $\Delta\delta_{5'B}$ and $\Delta\delta_{3'B}$ are their ^{1}H CSP relative to the free (F) form for the 5′- and 3′-plane nucleotides, respectively.

K_D Analysis. Monte Carlo simulations were performed to estimate the error associated with the fitting of binding curves to measure K_D. Random noise distributed with a Gaussian profile (with mean about the measured CSP and standard deviation as 0.007 ppm, i.e., 5 Hz being the error on the chemical shift measurement) was generated and added to each data point in the fitting. Fitting was repeated 250 times to determine the fitting error associated with the K_D measurement. The nonlinear least-square minimization algorithm in the *Scipy* library (Python v3.8 script) was used for curve fitting. Equations mentioned above were implemented in two independent ways: one where each nucleotide was fitted individually and the other where global analysis of data from all 11 guanines was performed simultaneously.

***Taq* DNA Polymerase Stop Assay.** The *Taq* Polymerase stop assay was implemented using a previously reported procedure with slight modifications.[26] Appropriate concentrations of the template (1 μM) and FAM-labeled primer (2 μM) were mixed in an annealing buffer containing 5 mM Tris (pH 8.0), 10 mM NaCl, and 0.1 mM EDTA. This template-primer solution in the annealing buffer was annealed by heating at 95 °C for 5 min followed by slow cooling over a period of 3−4 h. The annealed DNA solution was mixed with 1× polymerase buffer containing 50 mM Tris−HCl (pH 8.0), 0.5 mM DTT, 0.1 mM EDTA, 5 mM $MgCl_2$, 5 mM KCl for *c-MYC* and 10 mM KCl for the telomeric DNA template, 1 μg

μL-1 BSA in 5% glycerol, and 0.2 mM dNTPs. After this, appropriate concentrations of the **BIM-Pr1** ligand 0−50 μM for *c-MYC* and 0−120 μM for telomeric and mutated *c-MYC* template DNAs were used in a total volume of 10 μL. The reaction mixture was incubated for 30 min at room temperature. Finally, 0.5 U Taq DNA polymerase enzyme (Thermo Scientific) was added to the reaction mixtures and incubated at 55 °C for *c-MYC* and at 40 °C for the telomeric DNA over 30 min to initiate the primer extension reaction. The primer extension reactions were quenched by addition of 10 μL of a fast dye containing 80% formamide, 1× TBE, 50 mM EDTA (pH 8.0), and 0.025% each bromophenol blue. The extension products were examined on a denaturing 15% polyacrylamide gel having 7 M urea in 1× TBE (89 mM Tris−HCl and boric acid each, 2 mM EDTA, pH 8.2) running buffer. The gel was visualized by a Typhoon FLA 9500 phosphorimager (GE Healthcare). The bands on the gel were quantified with the help of Image J software. The IC_{50} values of the ligand were calculated using Origin 8.0 software by plotting the percentage of the stop product against ligand concentrations.

Cell Culture. HeLa and Lenti-X cell lines were cultured in Eagle's Minimum Essential Media (MEM) and in Dulbecco's modified Eagle's medium (DMEM), respectively, and supplemented with 5% sodium bicarbonate, 10% fetal bovine serum (HiMedia), and 1% antibiotic antimycotic Solution 100X liquid (HiMedia). Cells were maintained in a humidified atmosphere (Memmert, ICO) containing 5% CO_2 at 37 °C.

Cytotoxicity Assay. Cells were trypsinized from a T25 flask and counted using a hemocytometer. Around 10^4 cells were seeded in a 96-well plate and treated with a range of concentrations of **BIM-Pr1** (0−20 μM). After confluency reached 60−70%, cells were washed with phosphate-buffered saline (PBS) and incubated with a ligand for 24 h. Then, 100 μL of CellTitre Glo (Promega) was added and mixed on a rocker (Grant Bio, PMR 30) for 3−5 min and was allowed to stabilize for 10 min at room temperature. Luminescence was measured on a luminometer (Promega, GloMax 20/20). The percentage of viable cells was determined by the following equation[27]

$$\% \text{ of viability} = \left(\frac{L_{\text{treated cell}}}{L_{\text{untreated cell}}} \times 100 \right)$$

where $L_{\text{treated cell}}$ is the luminescent signal of treated cells and $L_{\text{untreated cell}}$ is the luminescent signal of untreated cells.

The percentage of viability was plotted against the concentration of the ligand, and the IC_{50} value was calculated using Prism-GraphPad by the following equation

$$\% \text{ live cells} = Y_{\text{min}} + \frac{Y_{\text{max}} - Y_{\text{min}}}{1 + 10^{(\log IC_{50} - X) \times \text{Hillslope}}}$$

where Y_{min} is the minimum % of live cells, Y_{max} is the maximum % of live cells, and X is the ligand concentration.

RNA Extraction for Real-Time PCR. Tyrpsinized cells from a T25 flask were counted and seeded at a density of 2×10^5 cells per well in six-well plates and allowed to adhere for 24 h. The cells were treated with **BIM-Pr1** (1 μM) and further incubated for 24 h. The next day, the media was discarded, and the cells were washed with PBS buffer (1 ml) and harvested by trypsinization. RNA was isolated using a GeneJET RNA purification kit (Thermo Scientific, K0731) according to the manufacturer's protocol. The lysis buffer containing cells was

vortexed and homogenized using a 20-gauge needle. The RNA was eluted from the column using 100 μL of nuclease-free water. The isolated RNA was quantified by a nanophotometer (IMPLEN) and used as a template in cDNA synthesis.

cDNA Synthesis. The cDNA synthesis was performed using a verso cDNA synthesis kit (Thermo Scientific, AB1453A) according to the manufacturer's protocol. A total of 1 ng of RNA template, 1× cDNA synthesis buffer (4 μL), 500 μM dNTP mix (2 μL), 500 ng of oligo dT primer (1 μL), RT enhancer (1 μL), verso enzyme mix (1 μL), and nuclease-free water were added, and the mixture was heated at 42 °C for 30 min for cDNA synthesis. The reaction mixture (20 μL) was then heated at 92 °C for 2 min for inactivation of the enzyme.

Real-Time PCR. The real-time quantitative PCR was performed on an AriaMx Real-Time PCR system (Agilent Technologies) using the Brilliant III Ultra-Fast SYBR Green QPCR master mix (Agilent Technologies, Catalog No. 600882). The forward and reverse primers used in the experiment are shown in Table S5. The amount of cDNA was optimized by dilution to get a significant threshold value for both the housekeeping and the target gene within the range (40 cycles). The PCR sample (10 μL) contains 2× SYBR green master mix (5 μL), cDNA (1 μL), 0.4 μL of each primers (20 μM), and nuclease-free water (3.2 μL). The thermal cycle was programmed as follows: hot start at 95 °C for 3 mins, 40 cycles of denaturation at 95 °C for 30 s, annealing at 57 °C for 30 s, and elongation at 72 °C for 30 s.[28] The relative gene expression of the gene of interest, together with the housekeeping gene, β actin, was determined by the arithmetic calibrator $2^{(-\Delta\Delta Ct)}$ method.[29]

$$C_T = \text{threshold cycle}$$

$$\Delta C_T = \{C_T(\text{housekeeping gene}) - C_T (\text{target gene})\}$$

$$\Delta\Delta C_T = \{\Delta C_T(\text{treated}) - \Delta C_T (\text{untreated})\}$$

First, the threshold values for both housekeeping and target genes were obtained from the experiment. Each sample was run in triplicate from three independent experiments. Error bars represent the standard deviations derived from three independent experiments.

The statistical analyses employed to evaluate the level of gene of interest in treated and untreated cells were compared, and the *p*-value was calculated by the *t*-test using GraphPad Prism 6. For the analysis, *p*-values less than 0.05 were considered significant.

Computational Methods. The initial structure of the ligand (**BIM-Pr1**) was prepared using the GaussView 6[30] interface of Gaussian 16. The ligand was subjected to initial optimization at the HF/6-31+G** theory level using Gaussian 16.[31] Dihedral scan was performed on the optimized structure using Gaussian 16. The dihedral angle formed by atoms C10−C5−C9−C15 (Figures S6 and S7) was used for defining the dihedral parameters. The planes formed by the maleimide moiety and one of the indolyl rings were considered for the definition of this dihedral angle. Scanning was done for a total of 36 steps with an increment of 10° each step. The structure corresponding to the energy minima of the dihedral scan was further optimized at the HF/6-31+G** level using Gaussian 16. The optimized ligand was docked with the NMR structure of *c-MYC* (PDB ID: 2L7V),[32] telomeric antiparallel (PDB ID: 143D),[33] and hybrid (PDB ID: 2JPZ)[34] using AutoDock 4.2.6[35] software. A grid box of 100 × 92 × 74 dimension with a

Scheme 1. Synthesis of Ligands BIM-Et, BIM-Pr1, and BIM-Pr2[a]
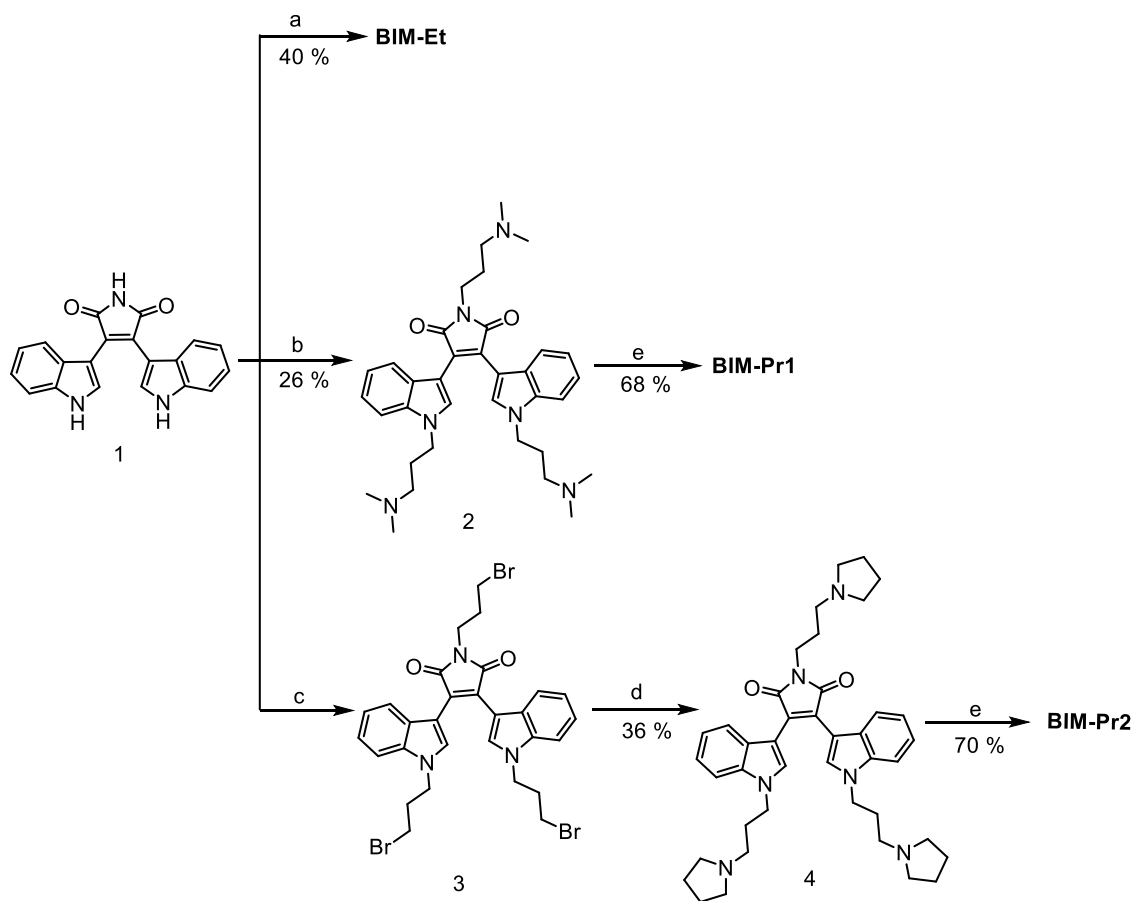
[a]Reagents and conditions: (a) 2-chloroethyl morpholine hydrochloride, Cs_2CO_3, THF, 1 h, MW: 250 W; (b) 3-chloro propyl N,N-dimethylamine hydrochloride, Cs_2CO_3, THF, reflux, 1 h, MW: 250 W; (c) 1,3-dibromopropane, THF, reflux, 1 h, MW: 250 W; (d) pyrrolidine, THF, reflux, 12 h; (e) HCl, DCM, RT, 6 h.

spacing of 0.375 Å was used to enclose the ligand and G4 DNA. The Lamarckian genetic algorithm was used to perform the docking with a maximum number of 25 000 000 energy evaluations. A total of 1000 independent structures of the ligand were generated. ESP charges were calculated for the selected docked conformers at the HF-6-31+G** theory level, and restraint electrostatic potential (RESP)[36] charges were fitted using the antechamber[37] module of AMBER 18.[38] The generalized AMBER force field (GAFF)[39] and the parmbsc1[40] force field were used to define the parameters of the ligand and DNA, respectively. The ligand–DNA complexes were prepared using the tleap interface of AMBER 18. The system was neutralized by adding K+ ions and was solvated using the TIP3P model of the water molecule in a 10 Å cuboid box. The system was subjected to 10 000 steps of minimization performed using the steepest descent method and then heated for 100 ps. The density equilibration of the system was carried out using the NPT ensemble for 100 ps. The system was further equilibrated on the NPT ensemble for 800 ps. Then, an unrestrained NPT production run was performed on the system for 1000 ns using the GPU accelerated version[41,42] of PMEMD in AMBER 18. The temperature was maintained at 300 K using the Langevin thermostat with a collision frequency of 2 ps^{-1} and a time constant of 1 ps. The pressure was maintained at 1 bar using a Berendsen barostat with a relaxation time of 2 ps.[43] The nonbonded interactions were

calculated using the particle mesh Ewald (PME) method with a cutoff of 10 Å. The hydrogen atoms were subjected to bond length constraints using the SHAKE algorithm. The coordinates of the trajectory were saved every 2 ps for further analysis. A cutoff of 3.5 Å and 135° were used for defining H-bonds, and a cutoff of 5 Å for electrostatic interactions. The root-mean-square deviation (RMSD), root-mean-square fluctuation (RMSF), H-bond, and electrostatic interaction distance calculations were performed using the CPPTRAJ[44] module of AmberTools19. Binding energy was calculated using the MM-PBSA[45] module of AMBER 18 for the last 20 ns of the simulation. UCSF chimera[46] was used for visualizing trajectories, and images were rendered using PyMOL (Schrodinger LLC.).

■ RESULTS AND DISCUSSION

Ligand Design and Synthesis. Indole and maleimide moieties are present in the biologically active natural product and FDA-accepted drugs, making them appropriate for G4 targeting.[47,48] Bisindolylmaleimide (**BIM**) scaffold, consisting of indole and maleimide moieties, is found in several lead molecules that act as protein kinase C inhibitors.[49] Herein, we have designed and synthesized a new class of trialkylated -**BIM** ligands (Figure 1). Due to their druglike properties and planar aromatic core, we hypothesized that these molecules could be used as promising G4 stabilizing ligands. These ligands were
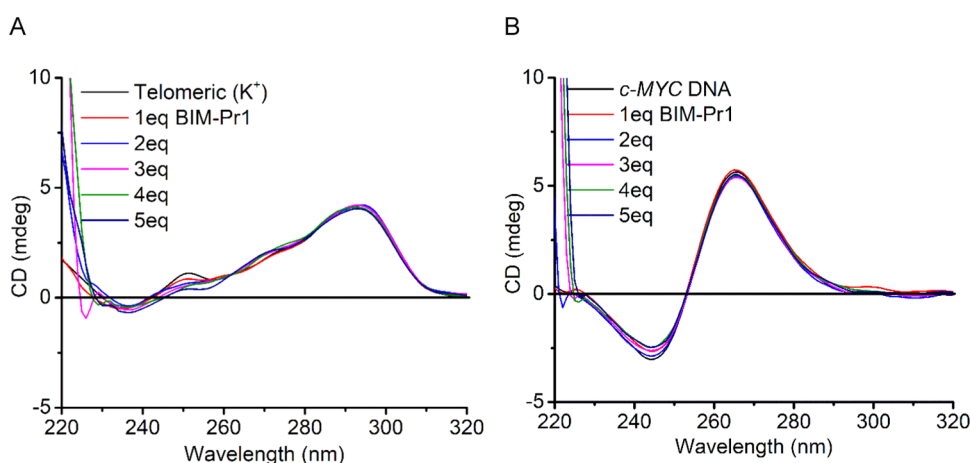
Figure 2. CD titration of *c-MYC* and telomeric G4 DNAs (10 μM in 10 mM lithium cacodylate buffer, pH 7.2) with **BIM-Pr1**: (A) telomeric DNA, 10 mM KCl, 90 mM LiCl; (B) *c-MYC* DNA, 1 mM KCl, 99 mM LiCl
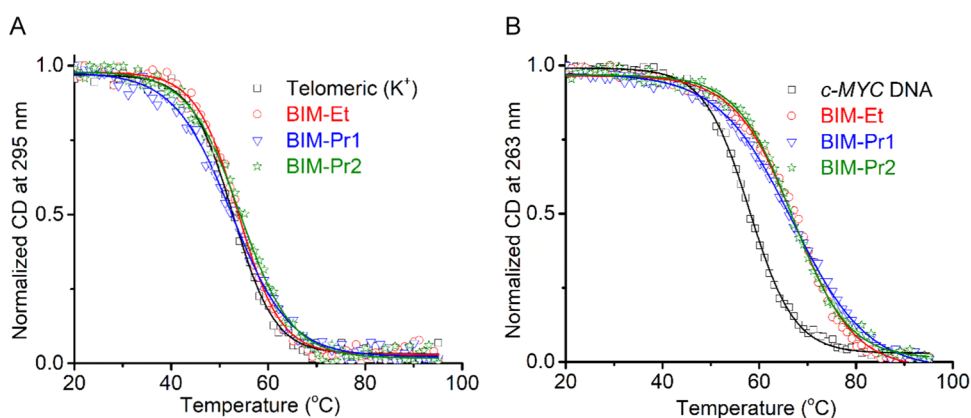

Figure 3. Normalized CD melting curves for telomeric G4 and *c-MYC* DNAs (10 μM in 10 mM lithium cacodylate buffer, pH 7.2) in the absence and presence of 5 molar equiv of ligand (A) telomeric DNA (10 mM KCl and 90 mM LiCl); (B) *c-MYC* (1 mM KCl and 99 mM LiCl).

surmised to stack on G4 tetrads, complemented by electrostatic interaction and hydrogen-bonding capabilities engineered in the side chains that potentially interact with the loop/grooves. The synthetic route followed to afford the designed ligands is shown in Scheme 1.

The synthetic route was embarked by preparing bisindolylmaleimide core **1**, using a previously reported method.[50] Compound **1** was then reacted with the 2-chloroethyl morpholine and 3-chloro propyl *N,N*-dimethylamine, under microwave conditions to access the desired ligand **BIM-Et** and compound **2** in 40 and 26% yields, respectively. Compound **1** was then further alkylated using 1,3-dibromopropane under microwave conditions to afford compound **3**. Compound **3** was then directly used without further purification to react with pyrrolidine to obtain compound **4**, having an overall yield of 36%. Compounds **2** and **4** were further protonated to furnish corresponding ligands **BIM-Pr1** and **BIM-Pr2** in 68 and 70% yields, respectively.

Titration Experiments with Circular Dichroism Spectroscopy. CD spectroscopy is routinely employed to evaluate the effect of metal ions and ligands on various topologies of the G4 DNA structure, with ellipticities at 240, 260, and 295 nm representing the structural signatures.[5] Upon addition of up to 5 molar equiv of any of the three ligands to telomeric G4 DNA, we observe that these signature ellipticities at 240, 260, and 295 nm are minimally perturbed, suggesting that the

telomeric DNA sequence retained its original mixture of topologies in the presence of K+ ions (Figures 2A and S1A,B, Supporting information). Similarly, titration of **BIM-Et**, **BIM-Pr1**, and **BIM-Pr2** with antiparallel topologies of telomeric DNA in Na+, *h-RAS1* (Figure S1C−H) and parallel topologies of c-MYC, *c-KIT1* (Figures 2B and S1I-M, Supporting information) minimally perturbed the ellipticities observed in the CD spectra even at 5 molar equiv, indicating the retention of the respective topologies. Overall, CD signatures in titration experiments revealed that the ligands, upon interacting with G4 DNAs, neither destroy the prefolded G4 topologies nor induce transition to other G4 topologies.

Thermal Melting Experiments with Circular Dichroism Spectroscopy. With no structural perturbations observed for the topologies in the presence of the BIM ligands, their thermodynamic stabilities were evaluated using thermal melting experiments using CD. The melting studies were monitored at the wavelength of maximum molar ellipticity obtained in CD spectra. Melting curves were recorded in the absence and presence of 5 molar equiv of **BIM-Et**, **BIM-Pr1**, and **BIM-Pr2** ligands. Telomeric DNA has the ability to form hybrid (3 + 1) and antiparallel topologies in the presence of K+ and Na+ ions, respectively. Thus, melting experiments were performed to evaluate the effect of thermal stabilization imparted on both of the topologies by the ligands at 295 nm (Figures 3A and S2A, Supporting information). The

Table 1. Thermal Stabilization of Various G4 and Duplex DNAs Obtained from CD Thermal Melting Experiments

ligands	[a]$\Delta T_{1/2}$ (°C)					
	c-KIT1	c-MYC	h-RAS1	Telomeric (K+)	Telomeric (Na+)	Duplex
BIM-Et	10.5 ± 0.2	8.2 ± 0.2	0.2 ± 0.2	−0.8 ± 0.3	0.8 ± 0.4	0.2 ± 0.4
BIM-Pr1	12.0 ± 0.1	8.5 ± 0.2	0.7 ± 0.4	0.3 ± 0.2	0.5 ± 0.2	1.2 ± 0.6
BIM-Pr2	11.2 ± 0.2	8.0 ± 0.3	−1.1 ± 0.2	0.5 ± 0.4	1.2 ± 0.2	−0.6 ± 0.5

[a]$\Delta T_{1/2}$ stands for the difference in the thermal melting [$\Delta T_{1/2} = T_{1/2}$ (DNA + 5 molar equiv ligand) - $T_{1/2}$ (DNA)]. The reported values average three different experiments with estimated standard deviations. All of the experiments were carried out using 10 μM quadruplex DNA or 15 μM duplex DNA in 10 mM lithium cacodylate buffer, pH 7.2. The $T_{1/2}$ values in the absence of ligands are 57.8 ± 0.2 for c-MYC DNA (1 mM KCl, 99 mM LiCl), 46.1 ± 0.1 for c-KIT1 DNA (10 mM KCl, 90 mM LiCl), 53.4 ± 0.2 for h-RAS1 DNA (50 mM KCl, 50 mM LiCl), 53.2 ± 0.4 for telomeric DNA in the K+ ion (10 mM KCl, 90 mM LiCl), 46.1 ± 0.3 for telomeric DNA in the Na+ ion (20 mM NaCl, 80 mM LiCl), and 62.0 ± 0.2 for duplex DNA (10 mM KCl, 90 mM LiCl).
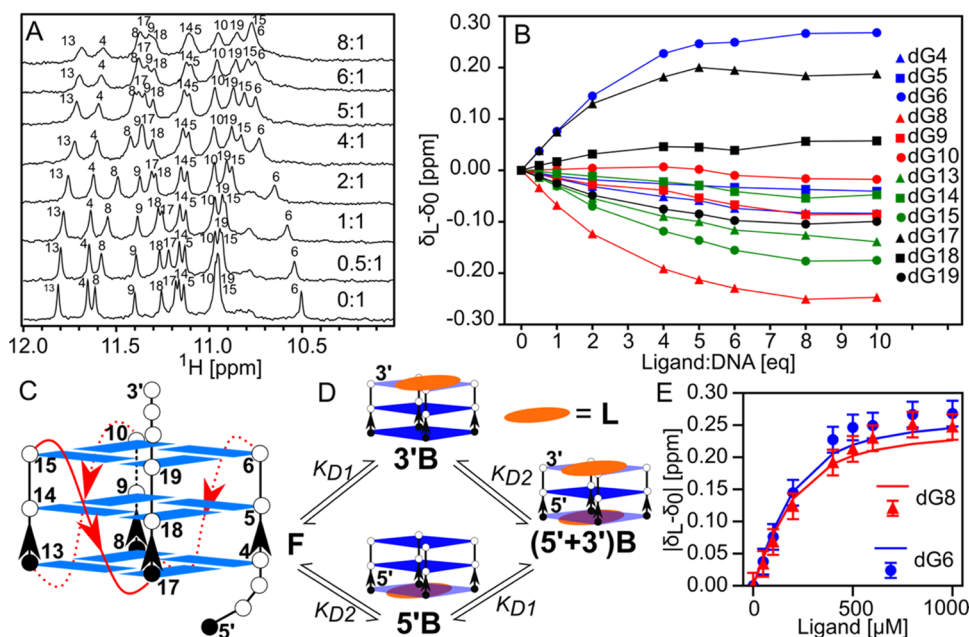

Figure 4. (A) Guanine ^{1}H imino resonances on titrating with the **BIM-Pr1** ligand; ratios indicate ligand:DNA concentration, with the DNA sample (100 μM, 25 mM potassium phosphate pH 7.0, 70 mM KCl) at 298 K. (B) Chemical shift differences between the ligand-bound form (δL) and the free form of DNA (δ0). Data points are marked as 5′-plane (▲), middle plane (■), and 3′-plane (●) and colored with strand-1 (blue), strand-2 (red), strand-3 (green), and strand-4 (black). Lines are drawn merely to connect data points and don't represent data fits. (C) Schematic of parallel G4 formed by c-MYC. (D) Binding model used for NMR-based titration studies, with F, 5′B, 3′B, and (5′ + 3′)B denoting the parallel folded, 5′ ligand stacked, 3′ ligand stacked, and both 5′ and 3′ ligand stacked forms, respectively. (E) Data points for the binding curves for dG6 (blue circle solid) and dG8 (red triangle up solid) nucleotides are displayed, and the global fit of absolute CSP as a function of ligand concentration providing K_{D1}/K_{D2} (75 ± 6 μM) is shown as a solid curve.

addition of any ligands displayed no significant changes ($\Delta T_{1/2}$ ~ 0.5−0.8 °C) in the melting temperature of telomeric G4 DNA under K+ conditions (Figure 3A and Table 1). Similarly, in Na+ conditions, only a minor change in the melting temperature ($\Delta T_{1/2}$ ~ 0.8−1.2 °C) was observed (Figure S2A, Supporting information, and Table 1). The melting temperatures of the parallel promoters G4 DNAs c-MYC and c-KIT1 were monitored at 263 nm (Figures 3B and S2B, Supporting information). In the case of c-KIT1 G4 DNA, adding 5 molar equiv of ligands displayed a significant increase in the melting temperature ($\Delta T_{1/2}$ ~10−12 °C) (Figure S2B, Supporting information and Table 1). Similarly, the addition of ligands to c-MYC G4 DNA showed an enhancement in the melting temperature ($\Delta T_{1/2}$ ~ 8.0−8.5 °C) (Figure 3B and Table 1). The thermal denaturation profile of h-RAS1 G4 DNA was monitored at 290 nm (Figure S2C, Supporting information), with almost no change observed in the melting temperature (Figure S2C, Supporting information and Table 1).

Thermal melting assays were also performed for these ligands against duplex DNA to verify their selectivity toward parallel G4s. The addition of ligands to duplex DNA displayed negligible changes in the melting temperature when monitored at 242 nm (Figure S2D, Supporting information and Table 1). Overall, melting studies reveal that the synthesized ligands preferentially stabilize the parallel G4s of c-MYC and c-KIT1 DNAs over duplex DNA and other nonparallel G4 topologies formed by h-RAS1 and telomeric DNA.

Titration Studies with NMR. The c-MYC DNA sequence folds into a unimolecular three-plane quadruplex in vitro in the presence of K+ ions (PDB ID: 1XAV).[51] Twelve well-resolved ^{1}H imino resonances (10−12 ppm, Figure 4A) agree with the reported chemical shifts of 1XAV.[51] Sequence-specific chemical shift assignments were verified with two-dimensional nuclear Overhauser effect spectroscopy (NOESY) and [13]C−[1]H heteronuclear single-quantum coherence spectra, confirming the formation of a parallel G4 (Figure 4C).[24] Upon titration
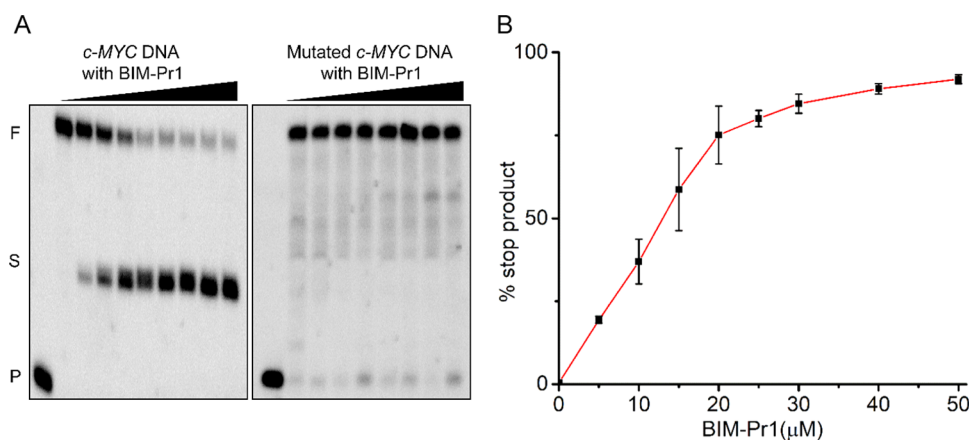
Figure 5. (A) Denaturing PAGE (15%, 7 M urea) of the *Taq* DNA polymerase stop assay of the *c-MYC* DNA template with an increasing concentration of **BIM-Pr1** (0−50 μM) and of the mutated *c-MYC* DNA template with **BIM-Pr1** (0−120 μM). (B) Plot of the percentage of the stop product against the increasing concentration of **BIM-Pr1**. P, S, and F denote the primer, the stop product, and the full-length product, respectively. Error bar represents the standard deviation from three independent experiments.

with **BIM-Pr1**, observation of 12 imino resonances indicates the ligand binding to *c-MYC* to be in the fast-intermediate NMR time scale (Figure 4A). In this exchange regime, chemical shift perturbation (CSP) as a function of ligand concentration provides an avenue to measure the equilibrium dissociation constant(s). Varying magnitudes of CSP are observed for multiple resonances as a function of ligand concentration and reaching saturation at ∼7−8 molar equiv of **BIM-Pr1** (Figure 4B). ^{1}H imino CSP mapped for each nucleotide indicates a 2:1 (**BIM-Pr1**: DNA) binding, with the two sites being 5′-plane and 3′-plane of the quadruplex, as observed for other ligands with *c-MYC* DNA.[32,52−54] Maximum absolute perturbation of ∼0.25 ppm is observed for dG6 (3′-plane) and dG8 (5′-plane) nucleotides (Figure 4B). dG15 and dG19 of the 3′-plane and dG13 and dG17 of the 5′-plane show a moderate perturbation of 0.1−0.2 ppm, while dG10 and dG4 nucleotides display minimal change until saturation (Figure 4B). These indicate that the ligand binding site is proximal to dG6, dG15, and dG19 on the 3′-plane and interacts minimally with dG10 (Figure 4B,C). Similar observations were made with the 5′-plane, as adjudged from dG8, dG13, and dG17, with the least magnitude of perturbation for dG4 (Figure 4B,C) plausibly due to the steric hindrance for dG4 from the 5′ terminal nucleotides dT1, dG2, and dA3.

Figure 4D provides the schematic of binding modes considered for the **BIM-Pr1** *c-MYC* DNA interaction, with K_{D1} and K_{D2} being dissociation constants for the 3′-plane and 5′-plane, respectively. The model assumes four states: free form (F), singly (5′B for the 5′-plane and 3′B for the 3′-plane), and doubly ((5′ + 3′)B) occupied sites. To the first order, CSPs of nucleotides present in 5′- and 3′-planes achieve 50% magnitude (relative to saturation) at similar ligand concentrations, pointing toward an independent binding to the two available faces of G4 (Figure 4B). Middle-plane nucleotides (dG5, dG9, dG14, dG18) are the least affected, pointing at minimal structural rearrangements following ligand binding on either of the tetrad pseudo-planes. This allows us to assume minimal structural alterations on the 5′-plane due to ligand binding at the 3′-plane and vice versa. Therefore, further analysis to measure binding affinities is performed by implementing a 2:1 independent site binding model (Figure 4D and Experimental Section), rationalized by the above observations. Individual fits for each residue indicate that K_{D1}

and K_{D2} are in the 15−120 μM range. Global analysis with all of the G-tetrad forming nucleotides indicates K_{D1} and K_{D2} to be 75 ± 6 μM (Figures 4E and S3). Since there are two independent binding sites, overall K_D turns out to be 38 ± 5 μM.

***Taq* DNA Polymerase Stop Assay.** The selectivity of the **BIM-Pr1** ligand toward parallel G4 DNA was further explored with the help of the *Taq* DNA polymerase stop assay,[26] where the addition of incremental concentrations of the **BIM-Pr1** ligand (0−50 μM) results in "stop" products in the reaction mixture containing the *c-MYC* DNA template (Figure 5A). The plot of the percentage of the stop product versus ligand concentration yielded an IC$_{50}$ value of ∼12.5 μM (Figure 5B). Contrastingly, such stop products are absent in the control experiments with mutated *c-MYC* DNA (that lacks G4 forming abilities) and telomeric DNA under similar reaction conditions (Figures 5A and S4, Supporting Information). These results show preferential stabilization of *c-MYC* over mutated *c-MYC* and telomeric G4 DNAs, which agrees with biophysical studies.

Cytotoxicity and Gene Downregulation Studies. A luciferase-based cell viability assay was performed to evaluate the antiproliferative activity of the ligand on normal and cancerous cell lines.[55] The cytotoxicity of the promising ligand **BIM-Pr1** was evaluated in HeLa (human cervical cancer cell) and Lenti-X (noncancerous human embryonic kidney cell) cell lines. The ligand exhibited a promising IC$_{50}$ value of 0.8 μM ± 0.05 in HeLa cell lines (Figure S5A, Supporting information), with Lenti-X cell lines exhibiting rather negligible cytotoxicity up to 20 μM of the ligand (Figure S5B, Supporting information).

To further study the effect of ligand **BIM-Pr1** on gene expression levels of *c-MYC*, mRNA transcription levels were quantified in the HeLa cell line using qRT-PCR methods.[29,56] Cells were treated with IC$_{50}$ **BIM-Pr1** ligand concentration for 24 h. The expression of *c-MYC* mRNA was normalized against the constitutively expressed housekeeping *β*-actin gene, which acted as a control. Results show that the *c-MYC* mRNA levels decrease by 50% compared to the untreated HeLa cells (Figure 6), indicating effective downregulation of the *c-MYC* gene expression upon **BIM-Pr1** ligand binding.

Molecular Modeling and Dynamics Studies. Molecular modeling and dynamics studies were carried out to profile the
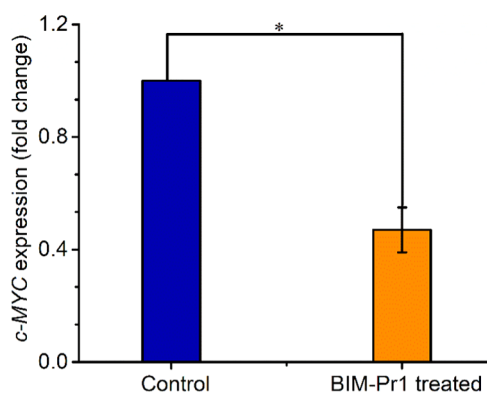
Figure 6. Effect of **BIM-Pr1** (1 μM) on the expression of the *c-MYC* gene in the HeLa cell line from qRT-PCR after 24 h of treatment. The fold change is calculated using the 2 ($-\Delta\Delta$Ct) method. Error bars represent the standard deviations acquired from three independent experiments. Asterisk * represents $p < 0.05$, which was considered significant difference as compared to untreated HeLa cells (control).

binding modes of the **BIM-Pr1** ligand with *c-MYC* G-quadruplex (G4) DNA at atomistic resolution. The ligand structure obtained after dihedral scanning and energy optimization (Figures S6 and S7, supporting information) was docked with the *c-MYC* G4 DNA. The docking reveals two binding poses for **BIM-Pr1** (Figure S8, Supporting Information), one stacking at the 3′-end and another at the 5′-end of the *c-MYC* G4 DNA, corroborating experimental observation of the 2:1 stoichiometric binding as revealed by NMR titration studies. Furthermore, a 1 μs unrestrained molecular dynamics simulation was performed, and the trajectory was used for analysis.

The root-mean-square deviation (RMSD) was calculated with respect to the first frame for heavy atoms of the backbone of the *c-MYC* DNA, 5′/3′ plane quartet, and **BIM-Pr1**. The RMSD of the backbone showed considerable fluctuations plausibly as a result of the conformational flexibility of the terminal nucleotides (Figure S9A, Supporting information). The RMSD of the G-quartets remained stable throughout the course of the simulation (Figure S9A, Supporting information). RMSD calculated for the **BIM-Pr1** ligand molecule at the 3′-end displayed a relatively higher magnitude of fluctuations than the 5′-end (Figure S9B,C, Supporting information). The per nucleotide root-mean-square fluctuation (RMSF) was calculated for elucidating the flexibility of the nucleotides of *c-MYC* DNA. The flanking nucleotides and loop nucleotides dT7, dT11, dA12, and dT16 showed fluctuations greater than 2 Å, whereas the G-quartet forming guanine nucleotides showed deviations less than 1.25 Å owing to its stability throughout the simulation (Figure S10, Supporting information). The 1 μs trajectory was clustered into five ensembles to group parts of simulations that share similar conformations. Two major clusters with populations of ~46% (cluster 1) and ~43% (cluster 2) were observed for the total time of the simulation (Figures 7A and S11A, Supporting information). On superimposition of cluster 1 and cluster 2, major differences were observed in the orientation of the 3′-end flanking nucleotide dA22 and the 5′-end flanking nucleotides dT1, dG2, and dA3 and the loop nucleotides dT7, dT11, dA12, and dT16 (Figure S12, Supporting information).

The representative structures of the major clusters revealed that **BIM-Pr1** at both the 3′-end and 5′-end exhibit altered orientations compared to the first frame of simulation (Figures 7B,C and S11B,C, Supporting information). The ligand displaced the flanking nucleotide dA22 at the 3′-end and stacked over the bottom quartet. Only one out of the two indolyl rings could partially stack over the G-quartet. The flanking 3′-end nucleotide dA22 gradually stacked over the dA21, enhancing the stabilizing interaction within the G4 DNA (Figures 7D and S11D, Supporting information). The ligand at the 5′-end showed stacking interactions, where one of the indolyl rings stacked over the flanking nucleotide dT1 and the other ring stacked over the G-quartet. The orientation of indolyl ring stacking above the G-quartet changed during the simulation, allowing the 5′-end nucleotide dA3 to stack over the dG4 nucleotide of the G-quartet, stabilizing the G4 DNA (Figures 7E and S11E, Supporting information).

To account for the noncovalent interactions, electrostatic and ion-induced dipole interactions of the protonated nitrogen of the ligand with the negatively charged phosphate backbone of the DNA G4 were analyzed (Table S1, Supporting information). At the 3′-end, the major interactions were of N6 interacting with OP2 of dT11 and N5 interacting with OP2 of the flanking nucleotide dA22 (Figure S13A,B, Supporting information). At the 5′-end, the major interactions were of N6 interacting with O4 (ion-induced dipole interaction) of the flanking nucleotide dT1 and N3 interacting with O2 (ion-induced dipole interaction) of the flanking nucleotide dT1 and with negatively charged phosphate OP1 of dA3 (Figure S13C,D, Supporting information). Several other electrostatic and ion-induced interactions were also observed for a small amount of time during the simulation. The electrostatic and ion-induced dipole interactions play an additional role in stabilizing the ligand−*c-MYC* complex.

The binding energy of the ligand−*c-MYC* complex was calculated using the MM-PBSA[41] module of AMBER 18 (Table S2, Supporting information). The Gibbs free energy for binding ($\Delta G^{\circ}_{binding}$) at 300 K was estimated to be - 56.62 ± 8.85 kcal/mol, indicating the high affinity of the ligand to *c-MYC* DNA. The enthalpic contributions account for the high affinity exhibited by the ligand. Thus, the MD simulation showed that **BIM-Pr1** has a stable dual binding mode with *c-MYC* DNA, which is in line with the NMR titration experiments. Both electrostatic and stacking interactions account for the overall stability of the ligand−*c-MYC* complex.

To probe the selectivity of the ligand toward the parallel topology, **BIM-Pr1** was docked with telomeric antiparallel (PDB ID: 143D) and telomeric hybrid (PDB ID: 2JPZ) G4 structures. The lowest energy docked conformers were selected for MD studies (Figure S14A,B). In the cases of both antiparallel and hybrid G4 structures, the ligand moved away from the quartet by the end of 100 and 300 ns simulations, respectively (Figures S15 and S16). Although the ligands did not fall off from the system, they do not exhibit proper binding modes (stacking or groove binding) with antiparallel and hybrid G4s. These observations are in line with the results from CD melting studies, which showed preferential stabilization of **BIM-Pr1** with parallel G4 structures. One likely reason for the selectivity could be the structural features of the ligand. The indole ring attached to the maleimide moiety exhibits a specific orientation with respect to each other (Figure S7). In the cases of both the antiparallel and hybrid topologies, the flanking nucleotides are more closed, leaving less space above the G-quartet for ligands to occupy. Overall,
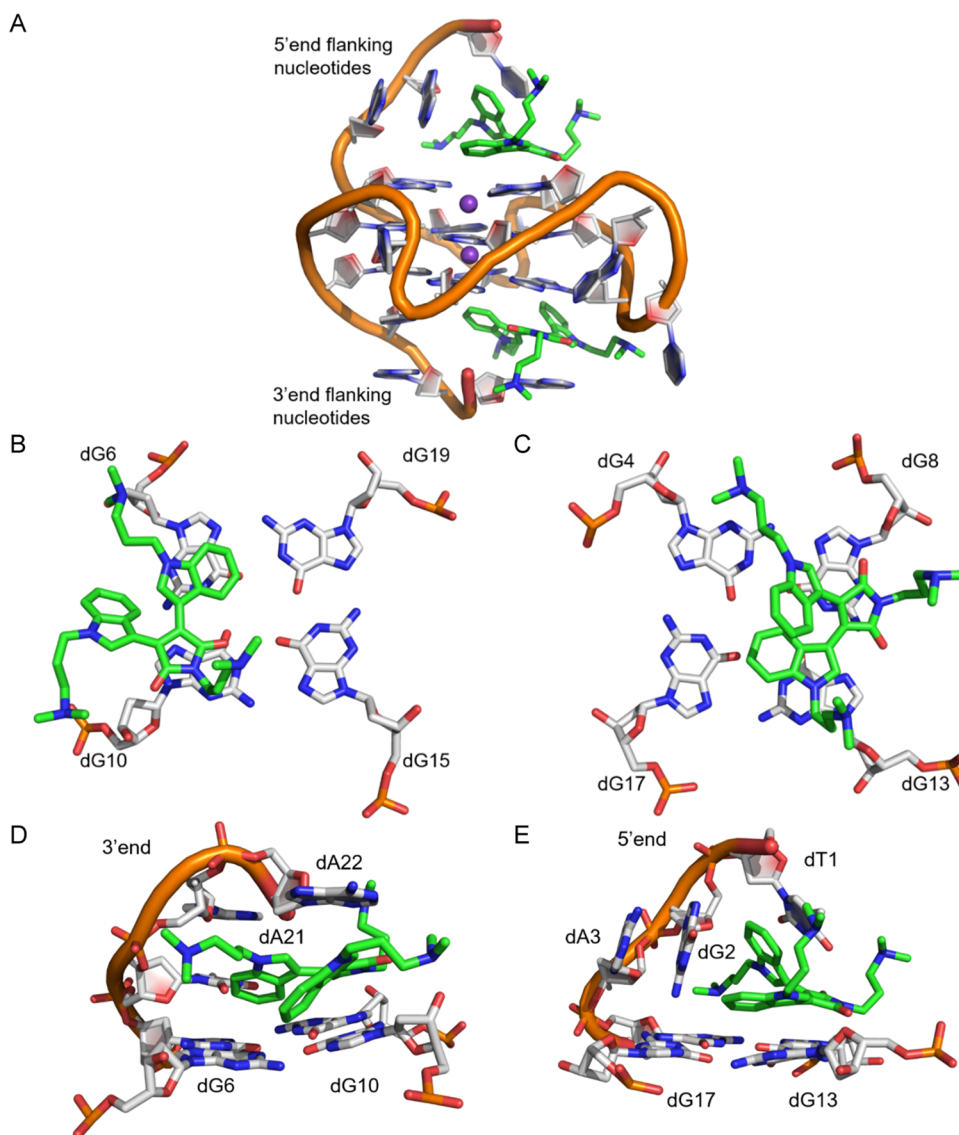
Figure 7. Representative structure of the major cluster 1 of the dual bound *c-MYC*/**BIMP-Pr1** ligand complex: (A) side view of cluster 1; (B) axial view of 3′-end binding of **BIM-Pr1** in cluster 1; (C) axial view of 5′-end binding of **BIM-Pr1** in cluster 1; (D) side view of 3′-end in cluster 1; and (E) side view of 5′-end in cluster 1. The K^+ ions are shown as purple spheres. The following color scheme has been used: carbon atoms, white; carbon atoms of the ligand, green; nitrogen atoms, blue; oxygen atoms, red; and phosphorus, reddish-orange.

the molecular modeling studies provided insights into the selective stabilization of ligands toward a parallel G4-topology.

SUMMARY AND CONCLUSIONS

We synthesized a series of bisindolylmaleimide-based ligands containing different side chains and performed biophysical and biological studies with various G4 and duplex DNAs. Studies have shown that the lead ligand **BIM-Pr1** preferentially stabilizes parallel *c-MYC* and *c-KIT1* promoter G4s by binding at two independent sites (5′ and 3′-end) of the *c-MYC* DNA with equal affinity. At the cellular level, **BIM-Pr1** is capable of downregulating the *c-MYC* gene expression. The electrostatic interaction of the positively charged side chains and the stacking of the aromatic units of the molecular scaffold with the G-quartet contribute to the G4 stabilization. Overall, due to their structural modifications, the studies established that these new molecular scaffolds have the potential for preferential binding toward parallel G4 topologies. These

scaffolds offer prospects for their future exploration for therapeutic and diagnostic research.

ASSOCIATED CONTENT

ⓢ Supporting Information

The Supporting Information is available free of charge at https://pubs.acs.org/doi/10.1021/acs.biochem.2c00116.

Supporting figures, oligonucleotide sequences used for studies, ^{1}H and ^{13}C NMR spectra of all new compounds (PDF)

AUTHOR INFORMATION

Corresponding Authors

Bharathwaj Sathyamoorthy − *Department of Chemistry, Indian Institute of Science Education and Research, Bhopal 462066, India;* ⓞ orcid.org/0000-0002-1568-2599; Email: bharathwaj@iiserb.ac.in

P. I. Pradeepkumar − *Department of Chemistry, Indian Institute of Technology Bombay, Mumbai 400076, India;* orcid.org/0000-0001-9104-3708; Email: pradeep@chem.iitb.ac.in

Authors

Satendra Kumar − *Department of Chemistry, Indian Institute of Technology Bombay, Mumbai 400076, India*

Rajesh Kumar Reddy Sannapureddi − *Department of Chemistry, Indian Institute of Science Education and Research, Bhopal 462066, India*

Chaitra S. Todankar − *Department of Chemistry, Indian Institute of Technology Bombay, Mumbai 400076, India*

R. Ramanathan − *Department of Chemistry, Indian Institute of Technology Bombay, Mumbai 400076, India*

Annyesha Biswas − *Department of Chemistry, Indian Institute of Technology Bombay, Mumbai 400076, India*

Complete contact information is available at:
https://pubs.acs.org/10.1021/acs.biochem.2c00116

Author Contributions

The manuscript was completed through the contributions of all authors. All authors have approved the final version of the manuscript.

Notes

The authors declare no competing financial interest.

REFERENCES

(1) Choi, J.; Majima, T. Conformational changes of non-B DNA. *Chem. Soc. Rev.* 2011, 40, 5893−5909.

(2) Guiblet, W. M.; DeGiorgio, M.; Cheng, X.; Chiaromonte, F.; Eckert, K. A.; Huang, Y. F.; Makova, K. D. Selection and thermostability suggest G-quadruplexes are novel functional elements of the human genome. *Genome Res.* 2021, 31, 1136−1149.

(3) Rhodes, D.; Lipps, H. J. G-quadruplexes and their regulatory roles in biology. *Nucleic Acids Res.* 2015, 43, 8627−8637.

(4) Jana, J.; Mohr, S.; Vianney, Y. M.; Weisz, K. Structural motifs and intramolecular interactions in non-canonical G-quadruplexes. *RSC Chem. Biol.* 2021, 2, 338−353.

(5) Ma, Y.; Iida, K.; Nagasawa, K. Topologies of G-quadruplex: Biological functions and regulation by ligands. *Biochem. Biophys. Res. Commun.* 2020, 531, 3−17.

(6) Balasubramanian, S.; Hurley, L. H.; Neidle, S. Targeting G-quadruplexes in gene promoters: a novel anticancer strategy? *Nat. Rev. Drug Discovery* 2011, 10, 261−275.

(7) Chen, Y.; Yang, D. Sequence, stability, and structure of G-quadruplexes and their interactions with drugs. *Curr. Protoc. Nucleic Acid Chem.* 2012, 50, 17.5.1−17.5.17.

(8) Agrawal, P.; Lin, C.; Mathad, R. I.; Carver, M.; Yang, D. The major G-quadruplex formed in the human BCL-2 proximal promoter adopts a parallel structure with a 13-nt loop in K + solution. *J. Am. Chem. Soc.* 2014, 136, 1750−1753.

(9) Tong, X.; Lan, W.; Zhang, X.; Wu, H.; Liu, M.; Cao, C. Solution structure of all parallel G-quadruplex formed by the oncogene RET promoter sequence. *Nucleic Acids Res.* 2011, 39, 6753−6763.

(10) Asamitsu, S.; Obata, S.; Yu, Z.; Bando, T.; Sugiyama, H. Recent progress of targeted G-quadruplex-preferred ligands toward cancer therapy. *Molecules* 2019, 24, No. 429.

(11) Cao, Q.; Li, Y.; Freisinger, E.; Qin, P. Z.; Sigel, R. K.; Mao, Z. W. G-quadruplex DNA targeted metal complexes acting as potential anticancer drugs. *Inorg. Chem. Front.* 2017, 4, 10−32.

(12) Che, T.; Wang, Y. Q.; Huang, Z. L.; Tan, J. H.; Huang, Z. S.; Chen, S. B. Natural alkaloids and heterocycles as G-quadruplex ligands and potential anticancer agents. *Molecules* 2018, 23, No. 493.

(13) Asamitsu, S.; Bando, T.; Sugiyama, H. Ligand Design to Acquire Specificity to Intended G-Quadruplex Structures. *Chem. - Eur. J.* 2019, 25, 417−430.

(14) Savva, L.; Georgiades, S. N. Recent developments in small-molecule ligands of medicinal relevance for harnessing the anticancer potential of G-quadruplexes. *Molecules* 2021, 26, No. 841.

(15) Chaudhuri, R.; Bhattacharya, S.; Dash, J.; Bhattacharya, S. Recent update on targeting c-MYC G-quadruplexes by small molecules for anticancer therapeutics. *J. Med. Chem.* 2021, 64, 42−70.

(16) Neidle, S. Quadruplex nucleic acids as novel therapeutic targets. *J. Med. Chem.* 2016, 59, 5987−6011.

(17) Diveshkumar, K. V.; Sakrikar, S.; Harikrishna, S.; Dhamodharan, V.; Pradeepkumar, P. I. Targeting Promoter G-Quadruplex DNAs by Indenopyrimidine-Based Ligands. *ChemMedChem* 2014, 9, 2754−2765.

(18) Dhamodharan, V.; Harikrishna, S.; Bhasikuttan, A. C.; Pradeepkumar, P. I. Topology specific stabilization of promoter over telomeric G-quadruplex DNAs by bisbenzimidazole carboxamide derivatives. *ACS Chem. Biol.* 2015, 10, 821−833.

(19) Diveshkumar, K. V.; Sakrikar, S.; Rosu, F.; Harikrishna, S.; Gabelica, V.; Pradeepkumar, P. I. Specific stabilization of c-MYC and c-KIT G-quadruplex DNA structures by indolylmethyleneindanone scaffolds. *Biochemistry* 2016, 55, 3571−3585.

(20) Pany, S. P. P.; Bommisetti, P.; Diveshkumar, K. V.; Pradeepkumar, P. I. (2016) Benzothiazole hydrazones of furylbenzamides preferentially stabilize c-MYC and c-KIT1 promoter G-quadruplex DNAs. *Org. Biomol. Chem.* 2016, 14, 5779−5793.

(21) Dhamodharan, V.; Pradeepkumar, P. I. Specific recognition of promoter G-quadruplex DNAs by small molecule ligands and light-up probes. *ACS Chem. Biol.* 2019, 14, 2102−2114.

(22) Wang, Y.; Silverman, S. K. Characterization of deoxyribozymes that synthesize branched RNA. *Biochemistry* 2003, 42, 15252−15263.

(23) Saha, R.; Verbanic, S.; Chen, I. A. Lipid vesicles chaperone an encapsulated RNA aptamer. *Nat. Commun.* 2018, 9, No. 2313.

(24) Reddy Sannapureddi, R. K.; Mohanty, M. K.; Gautam, A. K.; Sathyamoorthy, B. Characterization of DNA G-quadruplex Topologies with NMR Chemical Shifts. *J. Phys. Chem. Lett.* 2020, 11, 10016−10022.

(25) Arai, M.; Ferreon, J. C.; Wright, P. E. Quantitative analysis of multisite protein−ligand interactions by NMR: binding of intrinsically disordered p53 transactivation subdomains with the TAZ2 domain of CBP. *J. Am. Chem. Soc.* 2012, 134, 3792−3803.

(26) Kong, J. N.; Zhang, C.; Zhu, Y. C.; Zhong, K.; Wang, J.; Chu, B. B.; Yang, G. Y. Identification and characterization of G-quadruplex formation within the EP0 promoter of pseudorabies virus. *Sci. Rep.* 2018, 8, No. 14029.

(27) Nga, N. T. H.; Ngoc, T. T. B.; Trinh, N. T. M.; Thuoc, T. L.; Thao, D. T. P. Optimization and application of MTT assay in determining density of suspension cells. *Anal. Biochem.* **2020**, *610*, No. 113937.

(28) Carvalho, J.; Paiva, A.; Cabral Campello, M. P.; Paulo, A.; Mergny, J. L.; Salgado, G. F.; Queiroz uz, C.; Cruz, C. Aptamer-based targeted Delivery of a G-quadruplex Ligand in Cervical Cancer Cells. *Sci. Rep.* **2019**, *9*, No. 7945.

(29) Bookout, A. L.; Cummins, C. L.; Mangelsdorf, D. J.; Pesola, J. M.; Kramer, M. F. High-throughput real-time quantitative reverse transcription PCR. *Curr. Protoc. Mol. Biol.* **2006**, *73*, 1−15.

(30) Dennington, R.; Keith, T. A.; Millam, J. M. *GaussView 6.0. 16*; Semichem Inc.: Shawnee Mission, KS, USA, 2016.

(31) Frisch, M. J.; Trucks, G. W.; Schlegel, H. B.; Scuseria, G. E.; Robb, M. A.; Cheeseman, J. R.; Scalmani, G.; Barone, V.; Petersson, G. A.; Nakatsuji, H.; Li, X.; Caricato, M.; Marenich, A. V.; Bloino, J.; Janesko, B. G.; Gomperts, R.; Mennucci, B.; Hratchian, H. P.; Ortiz, J. V.; Izmaylov, A. F.; Sonnenberg, J. L.; Williams; Ding, F.; Lipparini, F.; Egidi, F.; Goings, J.; Peng, B.; Petrone, A.; Henderson, T.; Ranasinghe, D.; Zakrzewski, V. G.; Gao, J.; Rega, N.; Zheng, G.; Liang, W.; Hada, M.; Ehara, M.; Toyota, K.; Fukuda, R.; Hasegawa, J.; Ishida, M.; Nakajima, T.; Honda, Y.; Kitao, O.; Nakai, H.; Vreven, T.; Throssell, K.; Montgomery, J. A., Jr.; Peralta, J. E.; Ogliaro, F.; Bearpark, M. J.; Heyd, J. J.; Brothers, E. N.; Kudin, K. N.; Staroverov, V. N.; Keith, T. A.; Kobayashi, R.; Normand, J.; Raghavachari, K.; Rendell, A. P.; Burant, J. C.; Iyengar, S. S.; Tomasi, J.; Cossi, M.; Millam, J. M.; Klene, M.; Adamo, C.; Cammi, R.; Ochterski, J. W.; Martin, R. L.; Morokuma, K.; Farkas, O.; Foresman, J. B.; Fox, D. J. *Gaussian 16*, Rev. C.01; Gaussian Inc.: Wallingford, CT, 2016.

(32) Dai, J.; Carver, M.; Hurley, L. H.; Yang, D. Solution structure of a 2: 1 quindoline−c-MYC G-quadruplex: insights into G-quadruplex-interactive small molecule drug design. *J. Am. Chem. Soc.* **2011**, *133*, 17673−17680.

(33) Wang, Y.; Patel, D. J. Solution structure of the human telomeric repeat d[AG$_3$(T$_2$AG$_3$)$_3$] G-tetraplex. *Structure* **1993**, *1*, 263−282.

(34) Dai, J.; Carver, M.; Punchihewa, C.; Jones, R. A.; Yang, D. Structure of the Hybrid-2 Type Intramolecular Human Telomeric G-Quadruplex in K + Solution: Insights into Structure Polymorphism of the Human Telomeric Sequence. *Nucleic Acids Res.* **2007**, *35*, 4927−4940.

(35) Morris, G. M.; Huey, R.; Lindstrom, W.; Sanner, M. F.; Belew, R. K.; Goodsell, D. S.; Olson, A. J. AutoDock4 and AutoDockTools4: Automated docking with selective receptor flexibility. *J. Comput. Chem.* **2009**, *30*, 2785−2791.

(36) Fox, T.; Kollman, P. A. Application of the RESP methodology in the parametrization of organic solvents. *J. Phys. Chem. B* **1998**, *102*, 8070−8079.

(37) Wang, J.; Wang, W.; Kollman, P. A.; Case, D. A. Automatic atom type and bond type perception in molecular mechanical calculations. *J. Mol. Graph. Model.* **2006**, *25*, 247−260.

(38) Case, D. A.; Shalom, Y. B.; Broze, S. R.; Cerutti, D. S.; Cheatham, T. E.; Cruzeiro, V. W. D.; Darden, T. A.; Duke, R. E.; Ghoreishi, D.; Gilson, M. K. *AMBER 2018*; University of California: San Francisco, 2018.

(39) Wang, J.; Wolf, R. M.; Caldwell, J. W.; Kollman, P. A.; Case, D. A. Development and testing of a general amber force field. *J. Comput. Chem.* **2004**, *25*, 1157−1174.

(40) Ivani, I.; Dans, P. D.; Noy, A.; Pérez, A.; Faustino, I.; Hospital, A.; Walther, J.; Andrio, P.; Goñi, R.; Balaceanu, A.; Portella, G.; Battistini, F.; Gelpí, L. J.; González, C.; Vendruscolo, M.; Laughton, C. A.; Harris, S. A.; Case, D. A.; Orozco, M. Parmbsc1: a refined force field for DNA simulations. *Nat. Methods.* **2016**, *13*, 55−58.

(41) Götz, A. W.; Williamson, M. J.; Xu, D.; Poole, D.; Le Grand, S.; Walker, R. C. Routine microsecond molecular dynamics simulations with AMBER on GPUs. 1. Generalized born. *J. Chem. Theory Comput.* **2012**, *8*, 1542−1555.

(42) Le Grand, S.; Götz, A. W.; Walker, R. C. SPFP: Speed without compromise-A mixed precision model for GPU accelerated molecular dynamics simulations. *Comput. Phys. Commun.* **2013**, *184*, 374−380.

(43) Berendsen, H. J. C.; Postma, J. V.; Van Gunsteren, W. F.; DiNola, A. R. H. J.; Haak, J. R. Molecular dynamics with coupling to an external bath. *J. Chem. Phys.* **1984**, *81*, 3684−3690.

(44) Roe, D. R.; Cheatham, T. E. *J. Chem. Theory Comput.* **2013**, *9*, 3084−3095.

(45) Kollman, P. A.; Massova, I.; Reyes, C.; Kuhn, B.; Huo, S.; Chong, L.; Lee, M.; Lee, T.; Duan, Y.; Wang, W.; Donini, O.; Cieplak, P.; Srinivasan, J.; Case, D. A.; Cheatham, T. E. Calculating structures and free energies of complex molecules: combining molecular mechanics and continuum models. *Acc. Chem. Res.* **2000**, *33*, 889−897.

(46) Pettersen, E. F.; Goddard, T. D.; Huang, C. C.; Couch, G. S.; Greenblatt, D. M.; Meng, E. C.; Ferrin, T. E. UCSF Chimera-a visualization system for exploratory research and analysis. *J. Comput. Chem.* **2004**, *25*, 1605−1612.

(47) Chadha, N.; Silakari, O. Indoles as therapeutics of interest in medicinal chemistry: Bird's eye view. *Eur. J. Med. Chem.* **2017**, *134*, 159−184.

(48) Panov, A. A.; Simonov, A. Y.; Lavrenov, S. N.; Lakatosh, S. A.; Trenin, A. S. 3, 4-Disubstituted maleimides: synthesis and biological activity. *Chem. Heterocycl. Compd.* **2018**, *54*, 103−113.

(49) Gani, O. A. B. S. M.; Engh, R. A. Protein kinase inhibition of clinically important staurosporine analogues. *Nat. Prod. Rep.* **2010**, *27*, 489−498.

(50) Faul, M. M.; Winneroski, L. L.; Krumrich, C. A. A new, efficient method for the synthesis of bisindolylmaleimides. *J. Org. Chem.* **1998**, *63*, 6053−6058.

(51) Ambrus, A.; Chen, D.; Dai, J.; Jone, R. A.; Yang, D. Solution Structure of the Biologically Relevant G-Quadruplex Element in the Human *c-MYC* Promoter. Implications for G-Quadruplex Stabilization. *Biochemistry* **2005**, *44*, 2048−2058.

(52) Hu, M. H.; Yu, B. Y.; Wang, X.; Jin, G. Drug-like biimidazole derivatives dually target c-MYC/BCL-2 G-quadruplexes and inhibit acute myeloid leukemia. *Bioorg. Chem.* **2020**, *104*, No. 104264.

(53) Calabrese, D. R.; Chen, X.; Leon, E. C.; Gaikwad, S. M.; Phyo, Z.; Hewitt, W. M.; Alden, S.; Hilimire, T. A.; He, F.; Michalowski, A. M.; Simmons; Saunders, L. B.; Zhang, S.; Connors, D.; Walters, K. J.; Mock, B. A.; Schneekloth, J. S. Chemical and structural studies provide a mechanistic basis for recognition of the MYC G-quadruplex. *Nat. Commun.* **2018**, *9*, No. 4229.

(54) Liu, W.; Lin, C.; Wu, G.; Dai, J.; Chang, T. C.; Yang, D. Structures of 1: 1 and 2: 1 complexes of BMVC and MYC promoter G-quadruplex reveal a mechanism of ligand conformation adjustment for G4-recognition. *Nucleic Acids Res.* **2019**, *47*, 11931−11942.

(55) Riss, T.; Moravec, R.; Niles, A. Selecting cell-based assays for drug discovery screening. *Cell Notes* **2005**, *13*, 16−21.

(56) Bustin, S. A.; Mueller, R. Real-time reverse transcription PCR (qRT-PCR) and its potential use in clinical diagnosis. *Clin. Sci.* **2005**, *109*, 365−379.